A Model "Rebound" Mechanism of Hydroxylation by Cytochrome P450: Stepwise and Effectively Concerted Pathways, and Their Reactivity Patterns

François Ogliaro, Nathan Harris, Shimrit Cohen, Michael Filatov, Samuël P. de Visser, and Sason Shaik*

Contribution from the Department of Organic Chemistry and The Lise Meitner-Minerva Center for Computational Quantum Chemistry, Hebrew University, 91904 Jerusalem, Israel

Received June 7, 1999. Revised Manuscript Received June 5, 2000

Abstract: A two-state rebound mechanism of alkane hydroxylation by a model active species of the enzyme cytochrome P450 is studied using density functional theoretic calculations. Theory corroborates Groves's rebound mechanism (Groves, J. T. *J. Chem. Educ.* **1985**, *62*, 928), with a key difference, namely that in the two-state rebound the reactivity and product distribution result from the interplay of two reactive states of the active ferryl-oxene ($Por^{+\bullet}FeO$) species of the enzyme: one state is low-spin (doublet) and the other high-spin (quartet). Transition-state structures, intermediates, and product complexes are identified for the two states. The bond activation in either one of the two states involves a hydrogen abstraction-like transition structure. However, while in the high-spin state there forms a radical that has a significant barrier for rebound, in the low-spin state the rebound is virtually barrierless. Even though one cannot ignore incursion of a small amount of radicals in the low-spin state, it is clear that the radical has a significant lifetime mainly on the high-spin surface. The results are used to gain insight into puzzling experimental data which emerge from studies of ultrafast radical clocks (e.g., Toy, P. H.; Newcomb, M.; Hollenberg, P. F., *J. Am. Chem. Soc.* **1998**, *120*, 7719), vis à vis the nature the transition state, deduced from kinetic isotope effect measurements (Manchester, J. I.; Dinnocenzo, J. P.; Higgins, L. A.; Jones, J. P. *J. Am. Chem. Soc.* **1997**, *119*, 5069) and stereochemical scrambling patterns (Groves, J. T.; McClusky, G. A.; White, R. E.; Coon, M. J. *Biochem. Biophys. Res. Commun.* **1978**, *81*, 154). Understanding the electronic structure of the various species leads to a predictive structure−reactivity picture, based on the two-state reactivity scenario (Shaik, S.; Filatov, M.; Schröder, D.; Schwarz, H. *Chem. Eur. J.* **1998**, *4*, 193). The model makes it possible to predict the dependence of the relative rates of the two states, and of the corresponding steps as a function of the nature of the alkane, the resulting alkyl radical, and the binding capability of the thiolate proximal ligand of the active species.

Introduction

Alkane hydroxylation by cytochrome P450 is one of the most important processes by which biosystems metabolize toxic as well as endogenous compounds.[1] The mechanism of this reaction has been a subject of intense studies, but nevertheless, the mechanistic features remain disputed and raise questions. The consensus[2] mechanism, suggested by Groves et al.,[3] is the rebound mechanism shown in Scheme 1. This involves initial hydrogen abstraction from the alkane (RH) by the active ferryl-oxene species (**1**, $Por^{\bullet+}Fe^{IV}$-O), known also as Compound I,[1,2,4−8] followed by radical rebound on the ferryl-hydroxo intermediate, **2**, to generate the ferric−alcohol complex **3**, which then releases the alcohol and restores the resting state (the water complex). The rebound mechanism has gained support throughout the years from findings of rearranged alcohol products and other probes, such as trapping, which indicate the presence of a radical with a finite lifetime.[3,8−15] Additional indirect support for the rebound mechanism has recently been provided by the kinetic isotope effect (KIE) measurements of Dinnocenzo and Jones et al.,[16] who found that for a series of aryl-methanes, the

Scheme 1. Schematic Representation of the Rebound Mechanism

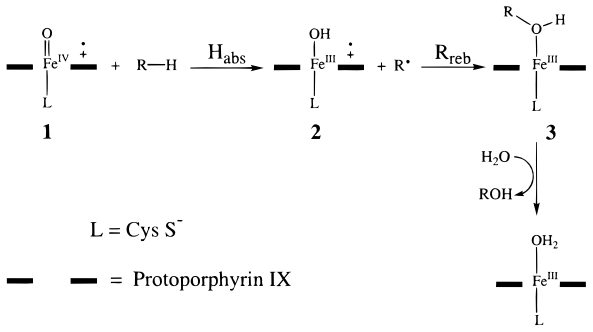

(1) Ortiz de Montellano, P. R., Ed. *Cytochrome P450: Structure, Mechanism and Biochemistry*, 2nd ed.; Plenum Press: New York, 1995.

(2) Sono, M.; Roach, M. P.; Coulter, E. D.; Dawson, J. H. *Chem. Rev.* **1996**, *96*, 2841−2887.

(3) (a) Groves, J. T. *J. Chem. Educ.* **1985**, *62*, 928−931. (b) Groves, J. T.; McClusky, G. A. *J. Am. Chem. Soc.* **1976**, *98*, 859−861. (c) Groves, J. T.; van der Puy, M. *J. Am. Chem. Soc.* **1976**, *98*, 5290−5297. (d) Groves, J. T.; Subramanian, D. V. *J. Am. Chem. Soc.* **1984**, *106*, 2177−2181.

(4) (a) For time-resolved X-ray characterization of the ferryl-oxene intermediate during camphor hydroxylation by $P450_{cam}$, see: Schlichting, I.; Berendzen, J.; Chu, K.; Stock, R. M.; Maves, S. A.; Benson, D. E.; Sweet, R. M.; Ringe, D.; Petsko, G. A.; Sligar, S. G. *Science* **2000**, *287* 1615−1622. For model compounds, see, for example: (b) Penner-Hahn, J. E.; McMurry, T. J.; Renner, M.; Latos-Grayzynsky, L.; Elbe, K. S. Davis, I. M.; Groves, J. T.; Dawson, J. R.; Hodgson, K. O. *J. Biol. Chem.* **1983** *258*, 12761−12764. (c) Boso, B.; Lang, G.; McMurry, T. J.; Groves, J. T. *J. Chem. Phys.* **1983**, *79*, 1122−1126. (d) Tsuchiya, S., *J. Chem. Soc., Chem. Commun.* **1991**, 716−717.

(5) Woggon, W.-D. *Top. Curr. Chem.* **1996**, *184*, 40−96.

10.1021/ja991878x CCC: $19.00
Published on Web 08/31/2000

KIEs of P-450 hydroxylation are virtually equal to those *of a corresponding hydrogen abstraction reaction* by tertiary butoxyl radical, thus implying isostructural transition states for the two processes.

The picture started to cloud, however, when radical clocks were used to time the rate of the rebound step.[2,17] Thus, the studies of Newcomb et al.[17] using ultrafast radical clocks have cast doubts on the presence of free radicals. Apparent lifetimes are too short to correspond to a real free radical intermediate (e.g., $\tau = 80-200$ fs)[17b,c,e] and have no correlation with independently clocked rearrangement lifetimes of the free radicals.[17a]

To elucidate the mechanism, Newcomb et al. have used clocks,[17c,e] such as **4** in Scheme 2a, that can undergo rearrangement in two distinct modes: one typical of a cyclopropyl methylene radical, and the other of a cyclopropyl methylene cation. Based on the rearranged products, an alternative mechanism has been suggested.[17c,e] This mechanism is based on "the two-oxidant hypotheses",[18] whereby cytochrome P450 operates via two oxidants as shown in Scheme 2b. The primary oxidant is ferryl-oxene species **1**, which is suggested[17e] to lead to an effectively concerted hydroxylation via oxygen insertion. The

Scheme 2. (a) A mechanistic probe, (b) Two P450 Oxidants, and (c) Scrambling Results in Norbornane Hydroxylation

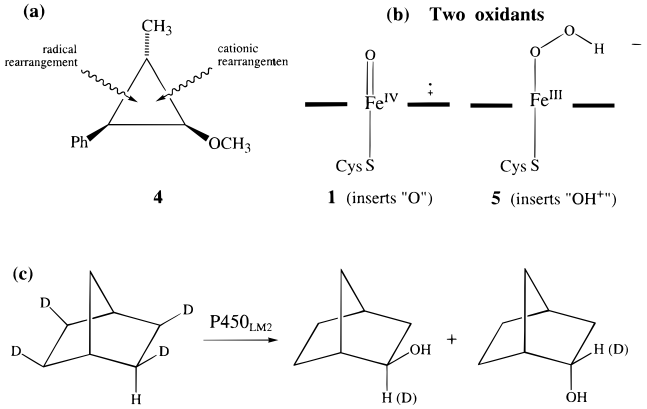

secondary oxidant, an iron-hydroperoxo species, **5**, inserts OH^+ and leads to the protonated alcohol which rearranges via anchimeric assistance in a manner typical of cationic species. The rearranged products that do not originate in carbocations are associated with apparent lifetimes which are too short to be assigned to free radicals.[17e] Therefore, these "radical-type" rearranged products are suggested to occur during collapse of the "O-insertion" transition state en route to the products, possibly via bifurcation of the potential surface, leading to two products from one transition state.[19]

While the evidence for cationic intermediates in the Newcomb clocks is compelling, the presence of radicals cannot altogether be dismissed. Evidence for radicals comes, for example, from the hydroxylation products obtained from deuterated norbornane in Scheme 2c.[20] In this case, both cytochrome[20a] $P450_{LM2}$ and artificial models[20b] of Compound I converge to the same conclusion, that a free norbornyl radical exists, which undergoes crossover from exo to endo epimers and gets hydroxylated from its two faces, thereby leading to both exo and endo alcohols with partial scrambling of the deuterium. The formation of endo alcohol does not concur with the sole presence of carbocations and is best understood by the assumption of free radical intermediary (the assumption of rearrangement via surface bifurcation[19] is attractive but still requires computational or experimental proof). More recent data reported by Hino and Dolphin[21] lead to the same conclusion: that intermediates exist during the hydroxylation and have a certain degree of freedom to undergo *rearrangement typical to radicals*. Additional complications which have to be considered are associated with the impact of the specific environment of the enzyme on the mechanism. Indeed, the fact that $P450_{cam}$ affords only exo alcohol products for deuterated camphor,[5,8,15,22] and the occasional dependence of the percentage of rearrangement on the identity of the isozyme,[17c,23] mean that the mechanism is not

(6) (a) Meunier, B. *Chem. Rev.* **1992**, *92*, 1411. (b) Dawson, J. H. *Science* **1988**, *240*, 433−439.

(7) For some leading references, see: (a) Loew, G. H.; Harris, D. L. *Chem. Rev.* **2000**, *100*, 407−419. (b) Loew, G. H.; Kert, C. J.; Hjelmeland, L. M.; Kirchner, R. F. *J. Am. Chem. Soc.* **1977**, *99*, 3534. (c) Hanson, L. K.; Chang, C. K.; Davis, M. S.; Fajer, J. *J. Am. Chem. Soc.* **1981**, *103*, 663−670. (d) Czernuszewicz, R. S.; Su, Y. O.; Macor, K. A.; Groves, J. T.; Spiro, T. G. *J. Am. Chem. Soc.* **1988**, *110*, 4158−4165.

(8) Groves, J. T.; Hang, Y.-Z. In *Cytochrome P450: Structure, Mechanisms and Biochemistry*, 2nd ed.; Ortiz de Montellano, P. R., Ed.; Plenum Press: New York, 1995; Chapter 1, pp 3−48.

(9) Groves, J. T.; Nemo, T. E. *J. Am. Chem. Soc.* **1983**, *105*, 6243−6248.

(10) Augusto, O.; Beilan, H. S.; Ortiz de Montellano, P. R. *J. Biol. Chem.* **1982**, *257*, 11288−11295.

(11) For summaries of evidence for radicals, see: (a) Dolphin, D. *Basic Life Sci.* **1988**, *49*, 491−500. (b) Ortiz de Montellano, P. R. *Trends Pharmacol. Sci.* **1989**, *10*, 354−359. (c) Ortiz de Montellano, P. R. *Acc. Chem. Res.* **1987**, *20*, 289−294.

(12) (a) Bowry, V. W.; Ingold, K. U. *J. Am. Chem. Soc.* **1991**, *113*, 5699−5707. (b) Bowry, V. W.; Lutztyk, J.; Ingold, K. U. *J. Am. Chem. Soc.* **1989**, *111*, 1927−1928.

(13) Ortiz de Montellano, P. R.; Stearns, R. A. *J. Am. Chem. Soc.* **1987**, *109*, 3415−3420.

(14) Atkinson, J. K.; Ingold, K. U. *Biochemistry* **1993**, *32*, 9209−9214.

(15) Gelb, M. H.; Heimbrook, D. C.; Malkonen, P.; Sligar, S. G. *Biochemistry* **1982**, *21*, 370−377.

(16) (a) Manchester, J. I.; Dinnocenzo, J. P.; Higgins, L. A.; Jones, J. P. *J. Am. Chem. Soc.* **1997**, *119*, 5069−5070. (b) The dimethylaniline substrates in ref 16a were suggested subsequently to undergo an initial electron transfer (Goto, Y.; Watanabe, Y.; Fukuzumi, S.; Jones, J. P.; Dinnocenzo, J. P. *J. Am. Chem. Soc.* **1998**, *120*, 10762−10763). This conclusion does not pertain, however, to the toluene, *p*-xylene, and benzyl alcohol species in ref 16a. Furthermore, all the model ferryl-oxene systems are much better acceptors than the P450 ferryl-oxene, so the results may not pertain at all to oxidation by P450.

(17) (a) Newcomb, M.; Le Tadic, M.-H., Putt, D. A.; Hollenberg, P. F. *J. Am. Chem. Soc.* **1995**, *117*, 3312−3313. (b) Newcomb, M.; Le Tadic-Beadatti, M.-H., Chestney, D. L.; Roberts, E. S.; Hollenberg, P. F. *J. Am. Chem. Soc.* **1995**, *117*, 12085−12091. (c) Toy, P. H.; Newcomb, M.; Hollenberg, P. F. *J. Am. Chem. Soc.* **1998** *120*, 7719−7729. (d) Atkinson, J. K.; Hollenberg, P. F.; Ingold, K. U.; Johnson, C.-C.; Le Tadic M.-H.; Newcomb, M.; Putt, D. A. *Biochemistry* **1994**, *33*, 10630−10637. (e) Newcomb, M.; Shen, R.; Choi, S.-Y.; Toy, P. H.; Hollenberg, P. F.; Vaz, A. D. N.; Coon, M. J. *J. Am. Chem. Soc.* **2000**, *122*, 2677−2686. (f) Newcomb, M.; Le Tadic, M.-H.; Putt, D. A.; Hollenberg, P. F. *J. Am. Chem. Soc.* **1993**, *117*, 3312−3313. (g) Newcomb, M.; Le Tadic, M.-H.; Chesteney, D. L.; Roberts, E. S.; Hollenberg, P. F. *J. Am. Chem. Soc.* **1995**, *117*, 12085−12091.

(18) (a) Vaz, A. D. N.; Pernecky, S. J.; Raner, G. M.; Coon, M. J. *Proc. Natl. Acad. Sci. U.S.A.* **1996**, *93*, 4644−4648. (b) Vaz, A. D. N.; McGinnity, D. F.; Coon, M. J. *Proc. Natl. Acad. Sci. U.S.A.* **1998**, *95*, 3555−3560. (c) Lee, K. A.; Nam, W. *J. Am. Chem. Soc.* **1997**, *119*, 1916−1922. (c) For a suggestion that hydroxylation proceeds via the hydroperoxo complex, see: Pratt, J. M.; Ridd, T. I.; King, L. J. *J. Chem. Soc., Chem. Commun.* **1995**, 2297−2298.

(19) (a) For discussions of bifurcation, see: Natanson, G. A.; Garrett, B. C.; Truong, T. N.; Joseph, T.; Truhlar, D. G. *J. Chem. Phys.* **1991**, *94*, 7875−7892. Baker, J.; Gill, P. M. W. *J. Comput. Chem.* **1988**, *9*, 465−475. Schlegel, H. B. *J. Chem. Soc., Faraday Trans.* **1994**, *90*, 1569−1574. See also the general discussion following this paper. (b) For a case of surface bifurcation in which one transition state, of ketyl anion radicals and alkyl halide reactant pairs, collapses into S_N2 and ET products, see: Shaik, S.; Danovich, D.; Sastry, G. N.; Ayala, P. Y.; Schlegel, H. B. *J. Am. Chem. Soc.* **1997**, *119*, 9237−9245.

(20) (a) Groves, J. T.; McClusky, G. A.; White, R. E.; Coon, M. J. *Biochem. Biophys. Res. Commun.* **1978**, *81*, 154−160. (b) Traylor, T. G.; Hill, K. W.; Fan, W.-P.; Tsuchiya, S.; Dunlap, B. E. *J. Am. Chem. Soc.* **1992**, *114*, 1308−1312.

(21) Hino, F.; Dolphin, D. *J. Chem. Soc., Chem. Commun.* **1999**, 629−630.

only sensitive to the probe substrate but may also depend on the specific enzyme used to carry the hydroxylation. Thus, the rearrangement question must be regarded also vis à vis the specific properties of the active species of the enzyme.

The Groves−Newcomb alternative mechanisms are both supported by good evidence and therefore pose an intellectually fascinating dilemma, perhaps exceedingly subtle for current experimental means. Theory may offer some insight in such a case, and this is the goal of the present paper. However, since the distinction between the two alternative mechanisms is still an awesome computational task, it is necessary to approach the problem in a stepwise manner, one mechanism at a time. In this paper we address the rebound mechanism of the ferryl-oxene species and try to resolve the dilemma associated with free radicals in the mechanism. Thus, we first address the following questions: Are radicals present or absent? If they are present, why do they possess apparent lifetimes that are too short to correspond to free radicals? What is the nature of bond activation process, and what is the relationship of the process in P450 to the hydrogen abstraction by tBuO•?[16] And finally, what mechanistic role might be played by the thiolate ligand in different isoforms of the enzyme?

Our preliminary studies have established two features which are helpful for the present study. First,[24] for a model system with a full cysteinato ligand and vinyl substituents on the porphyrin, and in a polarizing medium, the ground state of the iron hydroxo intermediate, **2** (Scheme 1), involves a porphyrin cation radical situation and Fe^{III}, which has a d^5 configuration. Second,[25] a free radical attack on the iron-hydroxo complex, **2**, involves both high-spin and low-spin rebound processes leading to corresponding spin varieties of the alcohol complexes. Since the ferryl-oxene species (**1**) itself has two low-lying states, the reaction commences with two states and continues as such. Therefore, *we are dealing here with a two-state reactivity (TSR) situation which involves high-spin and low-spin states, which jointly determine the mechanism and product distribution*.[26] Accordingly, the present paper addresses all the above mechanistic questions by establishing a complete rebound mechanism with transition states, clusters, and intermediates for the two reactive states, the high- and low-spin situations. A connection is drawn between the computational results and the experimental results with an attempt to account for patterns of structure−rearrangement relationships and to make some new predictions testable by experiment.

Methods

All calculations were done with GAUSSIAN98[27] as well as with the JAGUAR 3.5[28] packages. JAGUAR 3.5 offers the facility of an efficient initial guess methodology, which is important for convergence in computations of transition metal compounds. The hybrid (HF/DFT) density functional B3LYP calculation[29] was used. All calculations with GAUSSIAN98 were done with UB3LYP, the unrestricted open-shell version, while the JAGUAR 3.5 calculations employed the restricted version, ROB3LYP calculations. Since ROB3LYP cannot treat the low-spin-state situation of a multiplet state such as the ones used here (see later for Compound I, etc.), the JAGUAR calculations were done only for the high-spin surface.

Geometries for all the species in the high-spin and low-spin rebound processes were fully optimized without symmetry constraints. Whenever available, the geometries of the species and barrier heights in JAGUAR and GAUSSIAN are close. For geometry optimization we used the Los Alamos effective core potential coupled with the double-ζ LACVP basis set[30] on iron and the 6-31G basis for the rest of the atoms (hence, ECP+LACVP-6-31G). In a few cases, we employed a single-point calculation with a larger basis set. In the case of ferryl-oxene (**1** in Scheme 1), the results of larger basis sets (LACVP* and onward to 6-311+G*) corroborated the ECP+LACVP-6-31G results, and the small quantitative differences have no impact on the conclusions of the present paper. The state ordering of the iron hydroxo intermediate (**2** in Scheme 1) was verified with the ECP+LACV3P-6-311G* basis set.[30] The high- and low-spin hydrogen abstraction transition states (Figure 2) were calculated also with the LACVP* basis set (ECP+LACVP-6-31G*) and gave the same state ordering.

Even though basis set superposition error (BSSE) is small in DFT, the clusters found in this calculation are very weakly bound. Thus to avoid BSSE, we calculated bonding energies of a cluster relative to the fully optimized super molecule at large distances between the respective fragments (ca. 20 Å). The BSSE values are indeed small, e.g., 0.98 kcal/mol for the reactant cluster (^4C_R, Figure 1), but they are of the order of magnitude of the cluster stabilization energies.

The transition states for the high-spin process were ascertained with JAGUAR 3.5 by frequency calculations (ca. 256 CPU hours per job), while all high- and low-spin minima as well as transition states were characterized by frequency calculations using GAUSSIAN98.

Choice of Model Systems. To ascertain the most appropriate choice for Compound I,[4,5,7,8,31−33] we have calculated the four lowest electronic

(22) Mueller, E. J.; Loida, P. J.; Sligar, S. G. Twenty Five Years of $P450_{cam}$ Research. In *Cytochrome P450: Structure, Mechanism and Biochemistry*, 2nd ed.; Ortiz de Montellano, P. R., Ed.; Plenum Press: New York, 1995; Chapter 3, pp 83−124.

(23) (a) See, for example, differences for the Δ2E1 vs Δ2B4 and 2B1 isoforms, in the following: Toy, P. H.; Newcomb, M.; Coon, M. J.; Vaz, A. D. N. *J. Am. Chem. Soc.* **1998**, *120*, 9718−9719. While we note that this is not necessarily a typical result, it is nevertheless a pattern that requires consideration. (b) The dependence cannot be conveniently ascribed to enzyme-dependent steric restrictions within the enzyme's pocket. See, for example, evidence for free tumbling of adamantane/$P450_{cam}$, in the following: Lee, H.; Ortiz de Montellano, P. R.; McDermott, A. E. *Biochemistry* **1999**, *38*, 10808−10813. (c) For discussions on the variational character of the proximal and distal sites of the enzymes, see refs 36b,c.

(24) Filatov, M.; Harris, N.; Shaik, S. *Angew. Chem., Int. Ed.* **1999**, *38*, 3510−3512.

(25) Harris, N.; Cohen. S.; Filatov. M.; Ogliaro, F.; Shaik, S. *Angew Chem., Int. Ed.* **2000**, *39*, 2003−2007.

(26) (a) Shaik, S.; Filatov, M.; Schröder, D.; Schwarz, H. *Chem. Eur. J.* **1998**, *4*, 193−199. (b) Schröder, D.; Shaik, S.; Schwarz, H. *Acc. Chem. Res.* **2000**, *33*, 139−145.

(27) Frisch, M. J.; Trucks, G. W.; Schlegel, H. B.; Scuseria, G. E.; Robb, M. A.; Cheeseman, J. R.; Zakrzewski, V. G.; Montgomery, J. A., Jr.; Stratmann, R. E.; Burant, J. C.; Dapprich, S.; Millam, J. M.; Daniels, A. D.; Kudin, K. N.; Strain, M. C.; Farkas, O.; Tomasi, J.; Barone, V.; Cossi, M.; Cammi, R.; Mennucci, B.; Pomelli, C.; Adamo, C.; Clifford, S.; Ochterski, J.; Petersson, G. A.; Ayala, P. Y.; Cui, Q.; Morokuma, K.; Malick, D. K.; Rabuck, A. D.; Raghavachari, K.; Foresman, J. B.; Cioslowski, J.; Ortiz, J. V.; Stefanov, B. B.; Liu, G.; Liashenko, A.; Piskorz, P.; Komaromi, I.; Gomperts, R.; Martin, R. L.; Fox, J.; Keith, T.; Al-Laham, M. A.; Peng, C. Y.; Nanayakkara, A.; Gonzalez, C.; Challacombe, M.; Gill, P. M. W.; Johnson, B.; Chen, W.; Wong, M. W.; Andres, J. L.; Gonzalez, C.; Head-Gordon, M.; Replogle, E. S.; Pople, J. A. *GAUSSIAN98*; Gaussian, Inc.: Pittsburgh, PA, 1998.

(28) *JAGUAR 3.5*: Schrödinger, Inc.: Portland, OR, 1998. See: Vacek, G.; Perry, J. K.; Langlois, J.-M. *Chem. Phys. Lett.* **1999**, *310*, 189−194.

(29) (a) Stevens, P. J.; Devlin, F. J.; Chablowski, C. F.; Frisch, M. J. *J. Phys. Chem.* **1994**, *98*, 11623−11627. (b) Becke, A. D. *J. Chem. Phys.* **1993**, *98*, 5648−5652; **1992**, *96*, 2155−2160; **1992**, *97*, 9173−9177.

(30) Hay, J. P.; Wadt, W. R. *J. Chem. Phys.* **1985**, *82*, 299−308. Friesner, R. A.; Murphy, R. B.; Beachy, M. D.; Ringlanda, M. N.; Pollard, W. T.; Dunietz, B. D. Cao, Y. X. *J. Phys. Chem. A* **1999**, *103*, 1913−1928.

(31) For a synthetic P450 ferryl-oxene (Compound I) model, see: Wagenknecht, H.-H.; Woggon, W.-D. *Angew. Chem., Int. Ed. Engl.* **1997**, *36*, 390−393.

(32) For experiments to probe Compound I of $P450_{cam}$, see: (a) Egawa, T.; Shimada, H.; Ishimura, Y. *Biochem. Biophys. Res. Commun.* **1994**, *201*, 1464−1469. (b) Schlichting, I.; Berendzen, J.; Chu, K.; Stock, A. M.; Sweet, R. M.; Ringe, D.; Petsko, G. A.; Davies, M.; Mueller, E. J.; Benson, D.; Sligar, D. *FASEB J.* **1997**, *11*, A769. See recent publication in ref 4a. (c) Blake, R. C., II; Coon, M. J. *J. Biol. Chem.* ***1989***, *264*, 3694−3701.

(33) For additional computational results of Compound I, see the following. (a) For P450 models of Compund I, see refs 7a,b. (b) For Compund I without a proximal ligand, see: Ghosh, A.; Almløf, J.; Que, L., Jr. *J. Phys. Chem.* **1994**, *98*, 5576−5579. (c) Using thiolate and other proximal ligands for Compound I, see; Antony, J.; Grodzicki, M.; Trautwein, A. X. *J. Phys. Chem. A* **1997**, *101*, 2692−2701. (d) Using a variety of Compound I models, see: Filatov, M.; Harris, N. Shaik, S. *J. Chem. Soc., Perkin Trans. 2* **1999**, 399−410. (e) For P450 model with a methyl

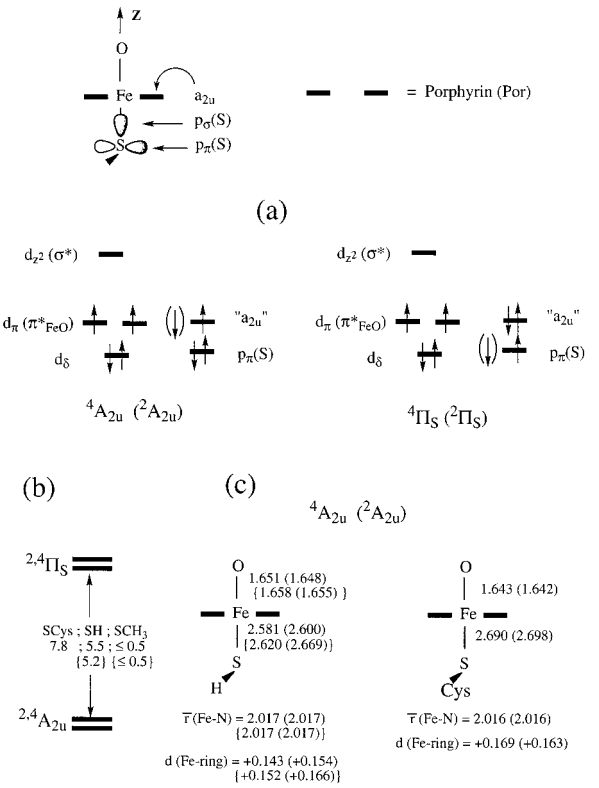

Figure 1. (a) Orbital diagrams and state assignments for electronic types of Compound I. (b) Energy separation of the states for $CysS^-$, HS^-, and CH_3S^- as proximal ligands. (c) Structural data for the $^{2,4}A_{2u}$ states for $CysS^-$ and HS^-. Positive *d*(Fe-ring) values correspond to iron above the porphyrin ring. The $\bar{r}$(Fe−N) quantity corresponds to an average iron−nitrogen distance in the porphyrin ring. Values in curly brackets correspond to geometries optimized with the extended all-electron basis set, 6-311+G*.

states for species **1** (Scheme 1) with L = SH^-, CH_3S^- and $CysS^-$, the latter being the full cysteinato ligand. We also used a variety of basis sets ranging from the simplest ECP+LACVP-6-31G to an all-electron basis set, 6-311+G*.[27] The four states were characterized by a careful analysis of the spin density distribution and of the natural orbitals of the four states in the three model species. The full results will be described elsewhere along with a bonding model for Compound I. At this point, suffice it to say that, based on the ordering of the four lowest lying states with the full cysteinato ligand, the simplest ligand, SH^-, is a faithful mimic (better than CH_3S^-) of the full ligand and will be used hereafter to model Compound I. The same conclusion was reached for the iron-hydroxo species (**2**, in Scheme 1), where a model with a full cysteinato ligand and vinyl substituents on the porphyrin established that L = SH^- is a good model for the full system.[24]

CH_4 was chosen as a model for the alkane, even though methane is not a P450 substrate. While this is a naive choice of substrate, its results can be used to model trends and to make predictions on relevant data. With these two model systems, we studied the hydroxylation process in the rebound mechanism shown in Scheme 1.

Location of Critical Structures for the Rebound Mechanism. An initial scan of the potential energy surfaces for C−H bond activation was carried out for the four low-lying states (see Figure 1) of Compound I, along the H−CH_3 coordinate, while all other degrees of freedom were optimized in C_s symmetry constraints. Subsequent full geometry optimization without any symmetry constraints identified each of the critical points. An eigenvector following algorithm was used for the transition states. The geometry optimization was followed by frequency analysis of the transition states for the lowest high-spin and low-spin states (GAUSSIAN; ^4TS_H, 947*i* cm^{-1}, ^2TS_H, 762*i* cm^{-1}; JAGUAR; ^4TS_H, 1180*i* cm^{-1}). The high-spin species was characterized by both GAUSSIAN (UB3LYP) and JAGUAR 3.5 (ROB3LYP); the corresponding geometries and barrier heights for the two methods were virtually identical. As an example, the energies for ^4C_R and ^4TS_H (which are the cluster and transition state for bond activation in Figure 2) are the following: −1676.0255407 and −1675.98229534 hartree with ROB3LYP, and −1676.0326616 and −1675.9885373 hartree with UB3LYP.

As found in a preliminary study,[24] the region of the rebound phase is characterized by two closely lying electronic situations, $Por^{+\bullet}Fe^{(III)}$-OH and $PorFe^{(IV)}OH$ types. Since the ferric state, $Por^{+\bullet}Fe^{(III)}OH$, is more stable in a polarizing medium, this state was followed in the present calculation. However, since the calculations correspond to a situation in a vacuum, the two electronic states are close, and GAUSSIAN98 occasionally failed to remain on the ferric (Fe^{III}) state and converged to the ferryl state (Fe^{IV}). For this reason, we used JAGUAR,[28] which converges efficiently on the desired electronic solution of transition metal compounds. The high-spin rebound step (Scheme 1, step ii) was initially scanned along the H_3C-O coordinate (from 20 to 1.6 Å), resulting in an approximate transition structure. This was followed by full transition-state optimization and frequency analysis. The harmonic frequencies confirmed that the transition state is a first-order saddle point having exactly one imaginary vibration (447.6*i* cm^{-1}) corresponding to the expected mode along the reaction coordinate: the approach motion of the oxygen atom and the methyl carbon atom toward each other. Single-point calculation with GAUSSIAN using UB3LYP gave spin densities, charges, and rebound barrier similar to those found with ROB3LYP using JAGUAR 3.5 (for spin, charge, see Figure 4, below). The low-spin rebound process was followed with GAUSSIAN and converged on the correct solution. The energy was found to descended smoothly toward the low-spin alcohol.

Both quartet and doublet ferric−alcohol products were characterized with full geometry optimization and frequency analysis with UB3LYP as well as with ROB3LYP. A sextet ferric−alcohol exists too but is not the ground state of the complex, in accord with known experimental evidence for ferric complexes which contain a thiolate sixth ligand (see, e.g., refs 50b and 51a). Since our tests showed that the sextet surface is higher in energy throughout the rebound pathway, this state will not be discussed any further. *As such, we shall use the names "high-spin" for the quartet state and "low-spin" for the doublet state.*

Results

Reactants States: Compound I. Figure 1 shows the four low-lying electronic states of the ferryl-oxene, Compound I. In part (a) we show key orbitals and their occupancy in the various states. These are the four low-lying d orbitals (the fifth, d_{xy}, is too high and not shown) and two additional orbitals, labeled as a_{2u}[7,8,33] and p_π(S). The a_{2u} orbital is a mixed a_{2u}(Por)−p_σ(S) orbital with a′ symmetry[24] in C_s and no symmetry in C_1, but for brevity we call it a_{2u} after its parent porphyrin orbital, following the common nomenclature in the literature.[7] The second orbital is a p_π(S) orbital, localized primarily on the sulfur, mixed somewhat with the in-plane $d_\pi(\pi^*)$ ferryl orbital and termed p_π(S) for brevity, and was identified recently to be important for a Compound I model with L = CH_3S^-.[33e]

The four low-lying electronic states which typify Compound I are triradicaloids having a high-spin triplet pair in ferryl's (FeO) π^* orbitals and an additional electron which resides in a_{2u} or in p_π(S) orbitals, leading thereby to two state types; for convenience the former one is labeled as A_{2u} while the latter is labeled as Π_S. Each state exists in two spin multiplicities (S = $^3/_2$, $^1/_2$), quartet and doublet. Note that the FeO moiety has an electronic structure with two π^* electrons in a triplet relationship and its bonding is analogous to that of triplet dioxygen.[26] Since

mercaptide ligand, see: Green, M. T. *J. Am. Chem. Soc.* **1999**, *121*, 7939−7940. (f) CASSCF calculations of model HRP Compound I, see: Yamamoto, S.; Hiroshi, K. *Chem. Phys. Lett.* **1988**, *145*, 111−116. (g) For HRP model of Compound I, see: Kuramochi, H.; Noodleman, L.; Case, D. A. *J. Am. Chem. Soc.* **1997**, *119*, 11442−11451. (h) For an extended Hückel description of Compound I, see: Tatsumi, K.; Hoffmann, R. *Inorg. Chem.* **1981**, *20*, 3771−3784.

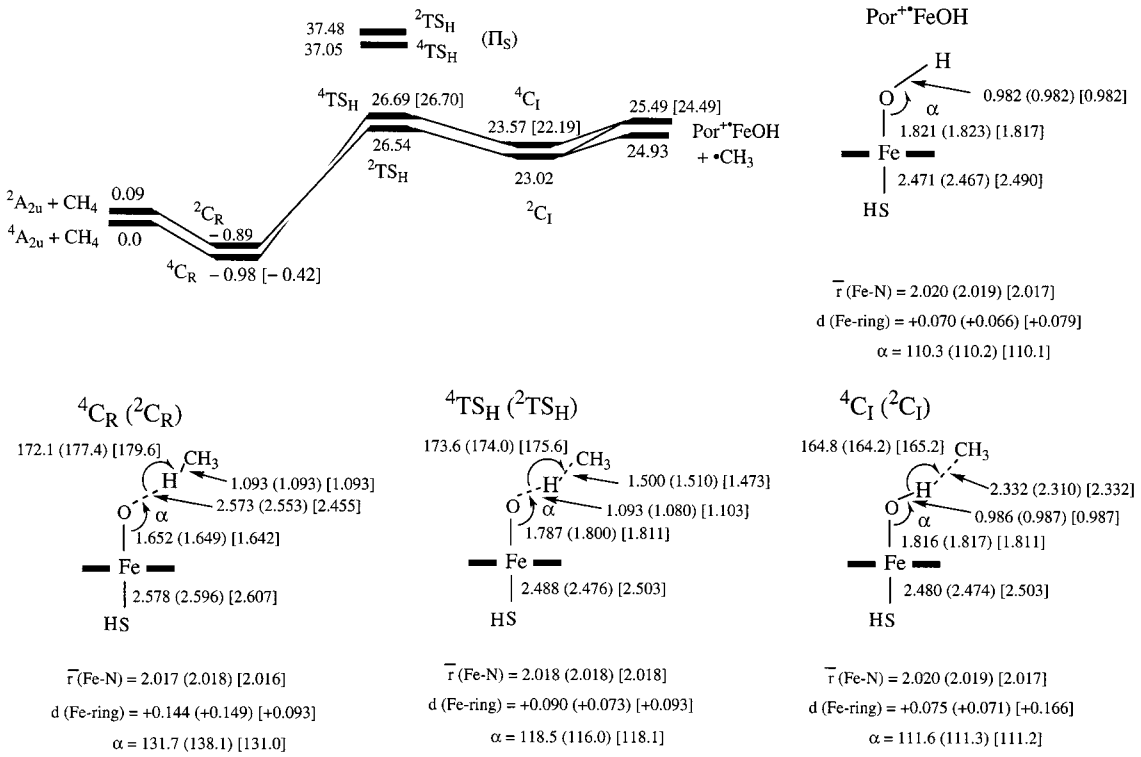

Figure 2. High-spin (quartet) and low-spin (doublet) energy profiles and critical species for the hydrogen abstraction phase of the rebound mechanism. Values in square brackets are high-spin ROB3LYP results; others are UB3LYP results. Also shown is the profile for the separation of the C_I intermediates.

the coupling between the π^* electrons and the third electron is weak, the quartet−doublet splitting for each state type is small, of the order of ±0.2 kcal/mol or smaller, irrespective of the basis set. This difference is much smaller than the inherent error of the DFT method, and one cannot therefore assign with certainty whether the spin multiplicity of the ground state is doublet or quartet. What the current level of theory permits us to say is that the ground state is a degenerate pair of quartet and doublet states, of either $^{4,2}A_{2u}$ or $^{4,2}\Pi_S$ type.

Part (b) of Figure 1 shows that the ordering of these states for cysteinato ($CysS^-$) and SH^- as ligands corresponds to $^{4,2}\Pi_S$ above $^{4,2}A_{2u}$ by ca. 6−8 kcal/mol. The third value belongs to CH_3S^- as a ligand, for which all the states are seen to be jammed within less than 1 kcal/mol, again irrespective of the basis set (or the Fe−S bond length). These results are insensitive to the basis set or to the precise geometry. The same results obtain even if one uses single-point calculations with the highest basis set (6-311+G*) on the geometries obtained by the simplest basis set (ECP+LACVP-6-31G) on all the species. It is reasonable to expect that the cysteinato ligand that bears an electron-withdrawing group is better represented by SH^-, which is a lesser electron donor in comparison with CH_3S^-. We conclude, therefore, that the HS^- ligand can model the cysteinato ligand in Compound I, and the entire study has been carried out with this ligand. Thus, *the active species of the P450 enzyme is characterized by a virtually doubly degenerate electronic ground state of the $^{4,2}A_{2u}$ variety*. It follows, therefore, that a minimum requirement for understanding the reactivity of the ferryl-oxene is the elucidation of the hydroxylation mechanism for these two states.

The key geometric details of the $^{4,2}A_{2u}$ states for the cysteinato and HS^- ligands are shown in part (c) of Figure 1 (for comparison with the same basis sets, for $L = SCH_3^-$ the primary geometric parameters are r_{FeO} (Å) = 1.643 (1.648); {1.643 (1.643)}, r_{FeS} (Å) = 2.764 (2.826); {2.909 (2.946)}). There is a generally good agreement with recent experimental determination of the structure.[4a] Thus, the FeO bond length is 1.64−1.65 Å, and the iron lies above the ring by 0.16−0.2 Å, as in the experimentally determined structure. However, the FeS bond length of 2.59−2.69 Å is longer than the experimental estimate of 2.3 ± 0.2 Å, and the difference may reflect the significant uncertainty in the experimental structure.

The Energy Profile for the Bond Activation Step. Figure 2 shows energetic and key geometric features of the critical species along the C−H bond activation step of the rebound mechanism. Initially, the two reactive states of the ferryl-oxene form very weakly bound clusters, $^{2,4}C_R$, in which the ferryl-oxene moiety is virtually the same as the free species. This is followed by a pair of closely lying transition states, $^{2,4}TS_H$, which, by natural orbital characterization, are clearly nascent from the A_{2u} states of the ferryl-oxene. Single-point calculation of these TS_H species with the LACVP* basis set keeps the same spin-state ordering and the species remain very close, within 0.41 kcal/mol. Above them there exist two additional transition states which correspond to hydrogen abstraction by the sulfur-localized states of the ferryl-oxene. The latter transition states are higher in energy relative to the A_{2u} derived ones and are therefore not described any further, even though we have characterized also the corresponding $C_R(S)$ and $C_I(S)$ clusters, which are ca. 5−7 kcal/mol higher than the ones shown in the figure.

The lower-lying transition states, $^{2,4}TS_H$, have structures of hydrogen abstraction transition states with an almost collinear arrangement of the O−H−C moiety and bond lengths reminiscent of other hydrogen abstraction transition states,[34] including that by $CH_3O^{\bullet}$.[35] In square brackets we show also the geometric features of the ^4TS_H species calculated by ROB3LYP using JAGUAR, and the similarity to the corresponding UB3LYP computed transition state is apparent in terms of both energies

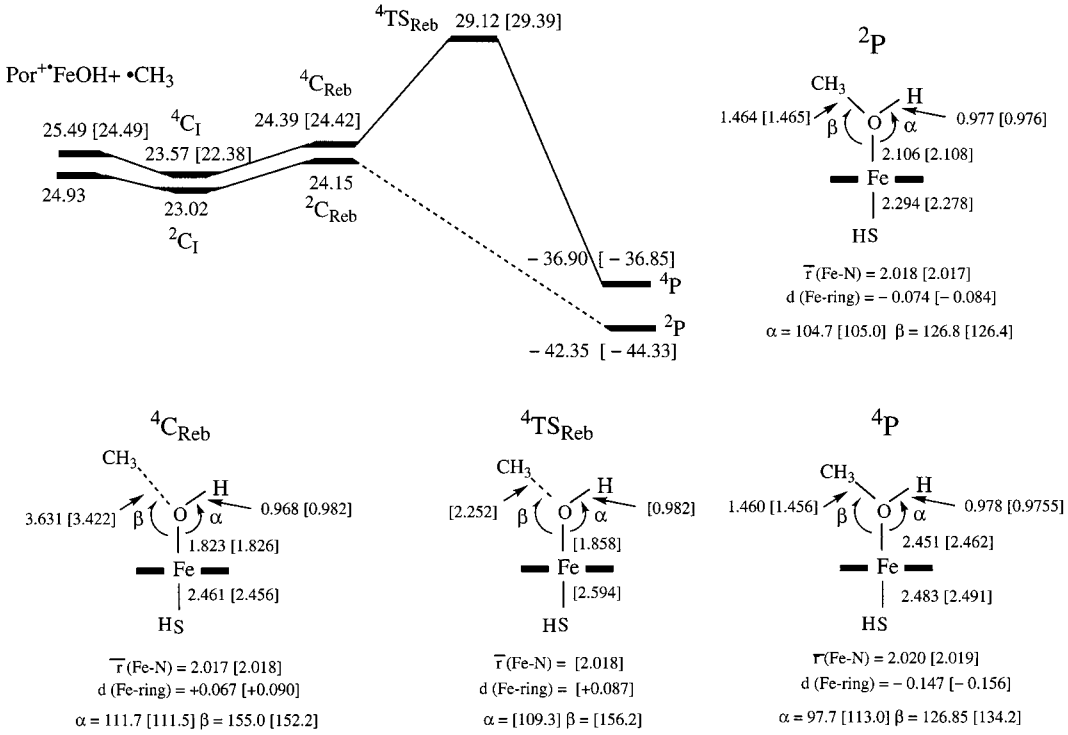

Figure 3. High-spin and low-spin energy profiles and critical species for the rebound phase of the rebound mechanism (C_{reb} are not real minima). Also shown are the profiles for separation of the C_I intermediate into ferryl-hydroxo and a free methyl radical. Values in square brackets are high-spin ROB3LYP results; others are UB3LYP results.

and geometries. Other geometric features of ^4TS_H and ^2TS_H are similar and involve the shortening of the Fe−S bond, lengthening of the Fe−O bond, minor breathing of the porphyrin, and a partial return of the Fe into the porphyrin plane.

The TS_H transition states lead into the corresponding intermediate clusters, $^{2,4}C_I$, where a methyl radical is still coordinated to the hydroxyl group of the ferryl-hydroxo complex, analogous to the finding of Basch et al.[34a] for CH_4 hydroxylation by a model of the MMO enzyme. Also shown in Figure 2 are the separations of the C_I intermediates to iron-hydroxo and free $CH_3^•$. There are two doublet species for three unpaired electrons. In the lower one (with datum shown in the figure), the spin-down electron is on the porphyrin. In the second one (not shown in the figure), the spin-down electron is on the methyl group. This second doublet state becomes degenerate with the quartet species at the dissociation limit of the iron-hydroxo and free $CH_3^•$. It is apparent that the doublet and quartet states which involve the methyl radical, and were discussed also in our preliminary study,[25] originate in the two states of the ferryl-oxene species.

Figure 3 shows two of the pathways available to the $^{2,4}C_I$ intermediate clusters. Thus, the two clusters may separate into a free $CH_3^•$ radical and iron-hydroxo complexes (see also Figure 2). The binding energy of the methyl is quite meager for both clusters, ca. 2 kcal/mol. Alternatively, the clusters can undergo a rebound reaction and produce the iron−alcohol products. In both cases, a methyl migration first takes place and orients the methyl group toward the vacant site of the hydroxo group, in a structure labeled as $^{2,4}C_{reb}$, corresponding to the "rebound-clusters" which *are not real minima* and are obtained by constraining the C−O−Fe−H dihedral angle to 180° along the C−O trajectory (followed from 20 Å toward 1.6 Å). As with the ^2C_I cluster here, too, there exist two doublet $^2C_{reb}$ species. In the lower one (with datum shown in the figure), the spin-down electron is on the porphyrin. In the second one (not shown in the figure and degenerate with $^4C_{reb}$), the spin-down electron is on the methyl group. The $^2C_{reb}$ species collapses into the low-spin alcohol product, virtually in a barrierless process.[25] In contrast, the high-spin species $^4C_{reb}$ has to traverse a barrier via the transition species $^4TS_{reb}$ to the high-spin alcohol product. The barrier for rebound is similar to the barriers calculated by Basch et al.[34a] for the MMO hydroxylation of methane. We note that the barriers (ROB3LYP and UB3LYP) for the high-spin rebound are higher than the energy required to free the radical. We cannot rule out generation of radicals on the low-spin surface, due to internal dynamics of ^2C_I, but the lack of a rebound barrier clearly implies a shorter, if ever finite, radical lifetime on the low-spin surface.

The geometries of the corresponding critical species are shown in the bottom part of Figure 3. It is apparent that the rebound transition structure, $^4TS_{reb}$, undergoes Fe−O and Fe−S bond lengthening relative to the $^4C_{reb}$ or ^4C_I clusters. This may be associated with the significant rebound barrier produced by the calculations.

Finally, the ground state of the product alcohol complex[36] is the low-spin doublet, ^2P, species irrespective of whether the

(34) (a) In MMO hydroxylation, see: Basch, H.; Mogi, K.; Musaev, D. G.; Morokuma, K. *J. Am. Chem. Soc.* **1999**, *121*, 7249−7256 (b) In hydrogen abstraction by a model ferryl-oxo species, see: Siegbahn, P. E. M.; Crabtree, R. H. *J. Am. Chem. Soc.* **1997**, *119*, 3103−3113. (c) In hydrogen abstraction by FeO^+, see: Yoshizawa, K.; Shiota, Y.; Yamabe, T. *Organometallics* **1998**, *17*, 2825−2831.

(35) Hrovat, D. A.; Borden, W. T. *J. Am. Chem. Soc.* **1994**, *116*, 6459−6460.

(36) (a) For the low-spin ground state of $P450_{cam}$−5-hydroxocamphor complex, see: Li, H.; Narashmhulu, S.; Havran, L. M.; Winkler, J. D.; Poulos, T. L. *J. Am. Chem. Soc.* **1995**, *117*, 6297−6299. (b) Lipscomb, J. D. *Biochemistry* **1980**, *19*, 3590−3599 (c) Unno, M.; Christian, J. F.; Benson, D. E.; Gerber, N. C.; Sligar, S. G.; Champion, P. M. *J. Am. Chem. Soc.* **1997**, *119*, 6614−6620. (d) For a recent experimental modeling of the water complex and a discussion of the role of protein in stabilizing the low-spin ground states, see: Aissaoui, H.; Bachmann, R.; Schweiger, A.; Woggon, W.-D. *Angew. Chem., Int. Ed.* **1998**, *37*, 2998−3002. See also the theoretical prediction: Harris, D.; Loew, G. H. *J. Am. Chem. Soc.* **1993**, *115*, 8775−8779.

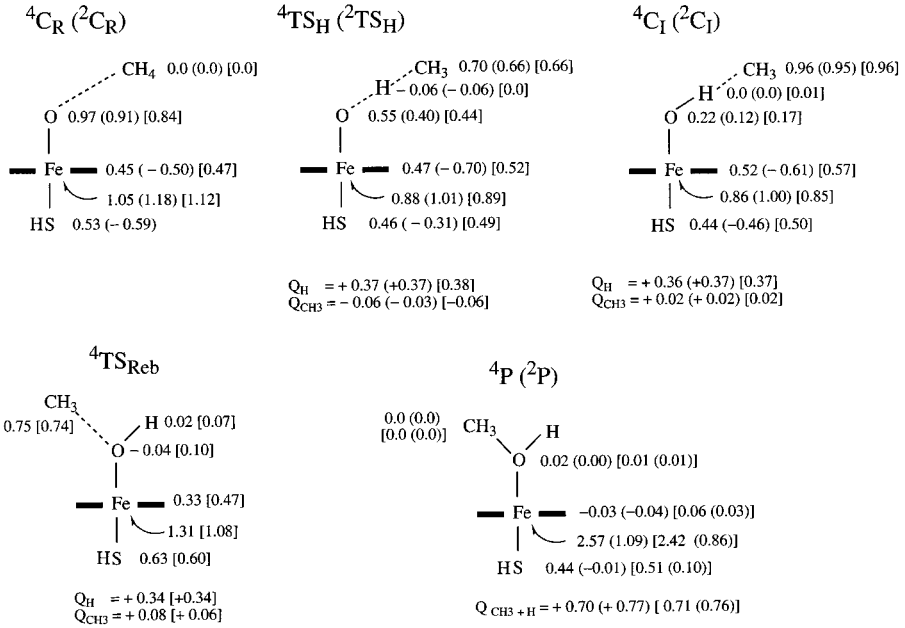

Figure 4. UB3LYP data of group spin densities for the various species in the rebound mechanism. In some cases, group charge density (*Q*) is also shown. In square brackets are ROB3LYP data for ^{4} TS_{reb}.

method used is ROB3LYP or UB3LYP. In each case, the low-spin ^{2}P alcohol exhibits shorter Fe−S and Fe−O bond lengths relative to the high-spin alcohol, ^{4}P. In both alcohol complexes the iron atom moves slightly below the porphyrin ring.

The spin density is the most diagnostic probe for the changes in the electronic structure along the reaction path. Figure 4 shows the spin densities for the various groups of the key critical species. In some cases group charges are also indicated. The spin densities on the ferryl-oxene moiety of the C_R species place about two units of spin on the FeO fragment, while the porphyrin and HS ligands carry together one unit of spin. This spin distribution is in accord with the triradicaloid electronic structure described in Figure 1, where the FeO fragment has a triplet dioxygen bonding type[26] with two unpaired spins, which are in turn weakly coupled to the electron spin in the "a_{2u}" type orbital.

Comparison of the $^{4,2}TS_H$ species to the $^{4,2}C_R$ species reveals two notable features. The TS_H species involve a significant charge transfer from the methane toward the ferryl-oxene moiety, and this charge transfer is slightly more pronounced in the low-spin TS relative to that in the high-spin species. Another feature is the spin density in the O−H−C moiety of the $^{4,2}TS_H$ species. Thus, the transition states exhibit positive spin densities on the heavy atoms flanking a negative spin density on the migrating hydrogen moiety (again, the high-spin case is similar to that reported by Basch et al.[34a]). This spin polarization is typical of transition states of a hydrogen abstraction process by a radical, as discussed later.

The rebound step exhibits a few interesting features. First, the correlation of the species, $^{4,2}TS_H \rightarrow {}^{4,2}C_R \rightarrow {}^{4,2}C_I$ is electronically smooth. The $^{4,2}C_I$ intermediate species resemble the electronic structure of the predecessor species, $^{4,2}TS_H$ and $^{4,2}C_R$, in the sense that they all involve an odd electron in the a_{2u} type orbital which has a mixed porphyrin−sulfur character, resulting thereby in spin distributions on the porphyrin and the sulfur orbitals ($a_{2u}-p_\sigma(S)$). Thus, the $^{4,2}C_I$ species can be described schematically as $Por^{+\bullet}Fe^{(III)}OH/CH_3^\bullet$ species. This ferric state is in accord with experimental datum of Groves et al.[37] for analogous $Por^{+\bullet}Fe^{(III)}OH$ species in solution. The alternative state of the $^{4,2}C_I$ intermediate, $PorFe^{(IV)}OH/CH_3^\bullet$, had been shown[24] to be less stable than the $Por^{+\bullet}Fe^{(III)}OH/CH_3^\bullet$ state when a cysteinato ligand and porphyrin substituents were used, and significantly less stable in a polarizing medium, which stabilizes preferentially the $Por^{+\bullet}Fe^{(III)}OH$ situation due to larger dipole moment and molecular polarizability. Thus, the σ-donor property of the thiolate raises the a_{2u} orbital and makes the $Por^{+\bullet}$-$Fe^{(III)}OH$ situation slightly better than the $PorFe^{(IV)}OH$ situation, and the polarizing medium further increases this preference. Nevertheless, it is not unlikely that in some cases the $PorFe^{(IV)}$-$OH/CH_3^\bullet$ species would compete with $Por^{+\bullet}Fe^{(III)}OH/CH_3^\bullet$ in the rebound step, making the process even more complex.[38,39]

The second feature in Figure 4 refers to the charge reorganization ensuing with the rebound event from the C_I species. Thus, the low-spin rebound involves conversion of a porphyrin cation radical situation in the cluster into an alcohol complex with a closed-shell porphyrin.[24,25] This is accompanied by an additional charge transfer from the methyl group into the iron-hydroxo moiety. The same trend is observed also for the high-spin process. However, in this latter case an important additional feature is the significant rise of the iron's spin density from 0.86 e in the cluster to 1.46 e [1.08 e] in $^4TS_{reb}$ and further to 2.26 e within a narrow range[25] in the vicinity of $^4TS_{reb}$, and all the way to 2.57 e [2.42 e] in the product ^{4}P. These electronic changes as well as the Fe−O and Fe−S bond elongation in the $^4TS_{reb}$ species will be discussed in the next section.

Discussion

The computed potential energy profiles for the rebound mechanism of methane hydroxylation exhibit a few key features. First, the hydroxylation mechanism involves two processes, nascent from the high-spin and low-spin electronic states of the ferryl-oxene. The two states cross along the bond activation

(37) Groves, J. T.; Gross, Z.; Stern, M. K. *Inorg. Chem.* **1994**, *33*, 5065−5072.

(38) For cases of both $Fe^{(III)}$ and $Fe^{(IV)}$ complexes, see: (a) Wolberg, A.; Manassen, J. *J. Am. Chem. Soc.* **1970**, *92*, 2982−2991. (b) Felton, R. H.; Owen, G. S.; Dolphin, D.; Fajer, J. *J. Am. Chem. Soc.* **1971**, *93*, 6332−6334. (c) Gans, P.; Buisson, G.; Duee, E.; Marchon, J.-C.; Erler, B. S.; Scholz, W. F.; Reed, C. A. *J. Am. Chem. Soc.* **1986**, *108* 1223−1234.

(39) For a theoretical analysis of the Fe(III)/Fe(IV) situation in a variety of complexes, see: Jones, D. H.; Hinman, A. S.; Ziegler, T. *Inorg. Chem.* **1993**, *32*, 2092−2095.

Scheme 3. **6a**, the Transition State for H Abstraction by Methoxyl Radical, with Group Spin Density Values (ρ) and Group Charges (Q); **6b**, the Corresponding Valence Bond Contribution for **6a**; **7a**, the O−H−C Portion of ^2TS_H; and **7b**, the Corresponding Valence Bond Contribution

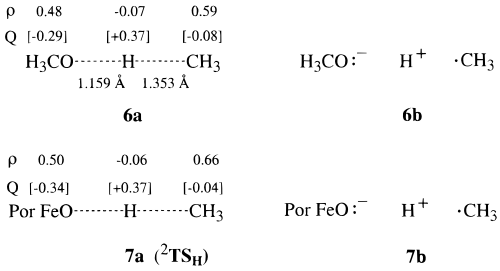

path[40a] and are nearly degenerate. Spin crossover will therefore be an essential feature of the two-state reactivity. This aspect of the reactivity, which is not treated in the present paper, will render the two states and their reactivity patterns virtually entangled. Furthermore, since the two surfaces are close in energy throughout the bond activation phase, we expect them to be competitive and to jointly affect the rate and product distribution. In other words, the hydroxylation mechanism by ferryl-oxene appears to be a two-state reactivity (TSR).[26,40b] It is in this context that we must discuss the various mechanistic features and their connection to experimental data.

First, we would like to understand the factors which control the barrier height for bond activation in the two states and to anticipate when one state will become dominant over the other. Second, we would like to understand the origins of the high-spin barrier in the rebound step as opposed to the lack thereof of a low-spin barrier. What possible impact might this have on the structure−reactivity patterns observed in the radical clock experiments? All these features will be discussed in conjunction with the electronic structure and the electronic reorganization of the two states as reflected in the Results section.

A. Electronic Features in the Different Phases of the Rebound Mechanism. A.1. The Hydrogen Abstraction Phase. The TS_H species in Figures 3 and 4 appear very similar in terms of geometry and spin/charge distribution to a hydrogen abstraction transition state. These salient features are summarized in Scheme 3 against a model hydrogen abstraction transition state, **6a**, by a methoxyl radical, computed in this work using UB3LYP on the ROB3LYP/6-31G* geometry. The similarity in geometry is apparent, but more telling are the spin density (ρ) and charge (Q) distributions. As seen in **6a**, the migrating hydrogen possesses a negative spin density, and this is diagnostic of three-electron/three-center transition states.[41] Also diagnostic of hydrogen abstraction transition states is the "polar effect"[42] that places a positive charge on the migrating hydrogen atom. This, in turn, can be associated with a contribution of the valence bond structure of the type shown in **6b** (Scheme 3).

Scheme 4. Orbital Diagrams for the Reactants and the Hydrogen Abstraction Intermediate Cluster[a]

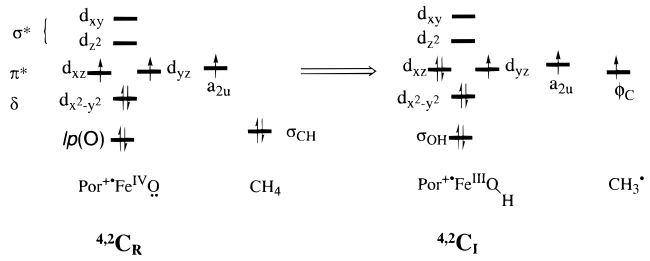

[a] The electrons in a_{2u} and ϕ_C can have spin-up or spin-down, corresponding to quartet and doublet spin situations, respectively. lp(O) is the oxygen's lone pair.

The spin and charge features of the O−H−C moiety in the ^2TS_H species from Figure 4 are summarized in **7a** in the scheme, and the analogy to **6a** is apparent. This analogy demonstrates that the oxygen atom of the ferryl unit acts *as though it were a radical center* that attacks the H−C bond, such that the O−H−C portion of the transition state acquires the characteristics of a three-electron/three-center species with an embedded polar effect, represented by the VB structure **7b** in Scheme 3. Interestingly, the kinetic isotope effect we calculated for the model reaction, due to **6a**, is 6.4. This value corresponds to a recently determined internal isotope effect for P450 hydroxylation of 6−8 for the Newcomb clocks[17d,e] and 5.9−7.4 with toluene and xylene.[16a,43] Thus, the contention by Dinnocenzo−Jones that the reaction of tBuO$^\bullet$ with alkanes can model important features of P450 hydroxylation appears quite reasonable.

Scheme 4 shows an alternative view of the polar effect in the hydrogen abstraction step, using orbital diagrams for the transformation of reactant to intermediate clusters (lp(O) is an oxygen lone-pair orbital). It is seen that the net effect is a formal loss of one electron by methane and a gain of one electron by the iron's d-block, which changes from d^4 to d^5. Thus, *the polar character of the TS_H species and in the hydrogen abstraction process is manifested as a formal one-electron oxidation of the alkane*. This is the first equivalent of the two-electron oxidation inherent in the net transformation of ferryl-oxene plus methane to a ferric−methanol complex.

A.2. The High-Spin Rebound Phase. Origins of the Barrier in the High-Spin Rebound. The rebound step starts from the intermediate clusters, $^{4,2}C_I$, which rearrange to $^{4,2}C_{reb}$ en route to rebound. There is no difference between the electronic features of the two types, so we will not be concerned with this aspect of the calculation. The essential feature to understand is the significant high-spin rebound barrier as opposed to the virtually barrierless low-spin rebound. Henceforth, we shall use the labels HS for high-spin and LS for low-spin.

Referring back to the $^{4,2}C_I$ clusters and the $^{2,4}P$ ferric−alcohol products in Figure 4, it is seen that the attacking $CH_3^\bullet$ radical and the porphyrin ring lose their initial spins in both the HS and LS rebounds. What makes the difference is the iron's spin density, which rises steeply on the HS path (from 0.86 to 2.57) but remains essentially constant (∼1.0) along the LS path. The

(40) (a) In Figure 2, the ground state of the ferryl-oxene is the high-spin state. However, the spin crossover will occur even if the ground state is the low-spin one, since the Fe−S bond is longer for the low-spin and undergoes shortening along the bond activation path. The bond shortening will induce spin-state interconversion. The Π_S states will mix with the A_{2u} states and provide the spin−orbit coupling needed to induce spin crossover. Precise details will be treated in a future paper. (b) Note, unlike in hydroxylations by FeO^+, here the low-spin process offers no energetic advantage over the high-spin process. The TSR characterization refers to the fact that both states determine product distribution.

(41) The negative spin density in three-electron/three-center species is well known, e.g., from ESR of ally radical. The same spin polarization appears in calculations (unrestricted Hartree−Fock, UDFT, CI, and VB) of transition states for hydrogen abstraction, e.g., in H_3. The origin of the spin polarization is well known. (a) For a VB explanation, see: Matsen, M. A. *Acc. Chem. Res.* **1978**, *11*, 387−392. (b) For an MO explanation, see: Borden, W. T. *Modern Molecular Orbital Theory for Organic Chemists*; Prentice-Hall: Englewood Cliffs, NJ, 1975; pp 265−271.

(42) See, for example: (a) Pross, A.; Yamataka, H.; Nagase, S. *J. Phys. Org. Chem.* **1991**, *4*, 135−140. (b) Wong, A. Pross, M. W.; Radom, L. *Isr. J. Chem.* **1993**, *33*, 415−425. (c) Fox, G. L.; Schlegel, H. B. *J. Phys. Chem.* **1992**, *96*, 298−302. (d) Reference 35. (e) Donahue, N. M.; Clarke, J. S.; Anderson, G. *J. Phys. Chem. A* **1998**, *102*, 3923−3933.

(43) Audergon, C.; Iyer, K. R.; Jones, J. P.; Derbyshire, J. F.; Trager, W. F. *J. Am. Chem. Soc.* **1999**, *121*, 41−47.

Scheme 5. Orbital Diagrams Showing the High-Spin (HS) and Low-Spin (LS) Rebound Processes To Form the Corresponding Alcohols, ^{4}P and ^{2}P

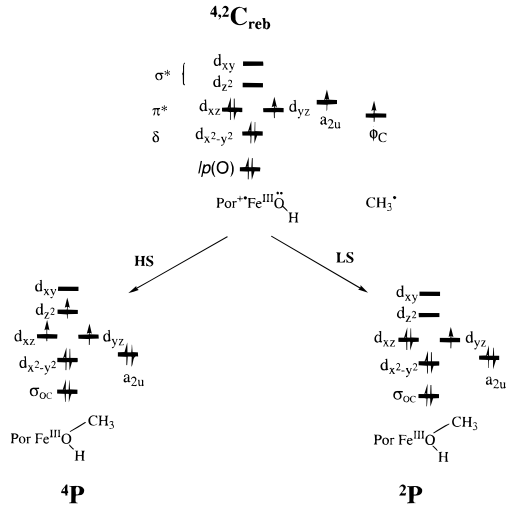

orbital diagrams for $^{4,2}C_{reb}$ and the alcohol products in Scheme 5 show the origins of this reorganization. Thus, initially in the clusters, the "a_{2u}" orbital[44] is singly occupied, and so is the orbital of the alkyl group (lp(O) is an oxygen lone-pair orbital). During the rebound, the "a_{2u}" orbital gets filled by an electron, formally provided by the alkyl radical $CH_3^\bullet$ which now participates in the newly formed σ_{OC} orbital. This is the second equivalent of the two-electron oxidation inherent in the net transformation of ferryl-oxene plus methane to a ferric−methanol complex.

While both HS and LS rebounds share this one-electron oxidation feature, there is a key difference between the two processes. Thus, to conserve a quartet spin during the rebound, the high-spin process must complement the porphyrin "reduction" by an excitation of an electron from the d_{xz} orbital to the high-lying (σ^* type) d_{z^2} orbital. Consequently, whereas in the $^4C_{reb}$(^4C_I) cluster all the unpaired electrons reside in relatively low-lying orbitals, in the HS-$^4TS_{reb}$ and in the corresponding HS ferric−alcohol product (^{4}P) one electron is excited to a higher-lying $\sigma^*(d_{z^2})$ orbital in order to conserve the total quartet spin. This additional excitation is accompanied by the increase of the spin density on the iron, as observed in our computations. Moreover, the $\sigma^*(d_{z^2})$ orbital involves antibonding interactions across the S−Fe−O axis, and consequently, its population during the HS rebound will be accompanied by elongation of the Fe−O and Fe−S bond lengths. These features can, in fact, be seen by comparing the structural data in Figure 3 for $^4TS_{reb}$ relative to the rebound cluster. *This excitation and loss of bonding are manifested as a barrier for the high-spin rebound process*.

A.3. The Low-Spin Rebound. While the barrier on the high-spin rebound has a clear electronic origin, the reason for the lack of barrier in the low-spin rebound process is still not apparent. Nor is it apparent what precisely is the role of the porphyrin cation radical situation (porphyrin "hole") or of the proximal thiolate ligand in mitigating the barrier. Scheme 6a shows a cartoon of the LS rebound process. Thus, initially the C−O linkage involves three electrons, one more than is required for making the C−O bond in the alcohol, while at the same time the porphyrin is missing one electron. At the end of the process, the porphyrin attains a closed shell and the C−O linkage becomes a two-electron bond.[45]

(44) For the Por$^{+\bullet}$Fe$^{(III)}$OH species, "a_{2u}" is a 60% mixture of porphyrin a_{2u}-type MO and 30% sulfur p_σ orbital (with small delocalization into the oxygen). In this case, too, our results[24] show that the SH$^-$ ligand is a better mimic than SCH_3^- for CysS$^-$.

Scheme 6. Features of the Low-Spin Rebound Phase[a]

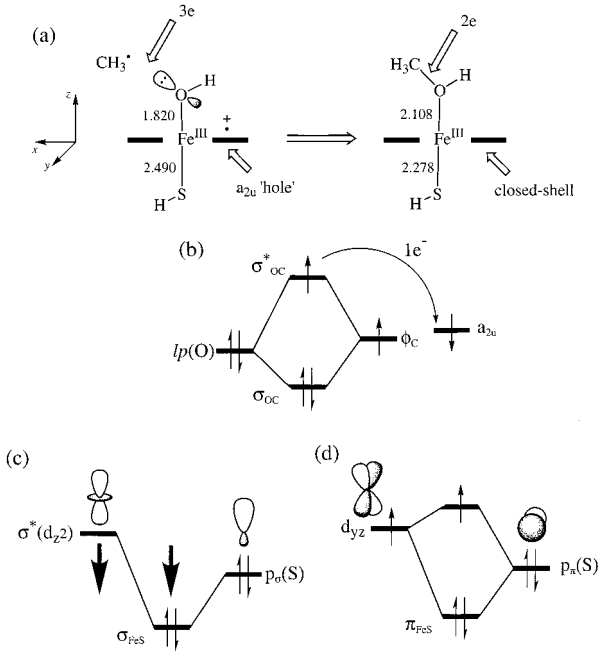

[a] (a) A cartoon showing the structural changes and the filling of the porphyrin hole by an electron shift formally from the radical. (b) The role of the porphyrin a_{2u} hole as an electron sink for the excess electron in the C−O linkage. (c) Illustration of the "push effect" of the thiolate. The heavy arrows show that the lowering of $\sigma^*(d_{z^2})$ causes a stronger interaction with the p_σ(S) orbital, thereby strengthening the Fe−S bond. (d) Strengthening of the π-back-bonding of the thiolate to the iron due to Fe−S shortening.

The Role of the Porphyrin "Hole". The orbital diagram in Scheme 6b projects the role of the porphyrin "hole". The initial C−O three-electron interaction (see Scheme 6a) develops into a bonding σ_{CO} orbital and an antibonding σ^*_{CO}. Initially, these three electrons are populated in the C−O linkage. As this interaction gets stronger it becomes repulsive due to the sharp rise of the antibonding σ^*_{CO} orbital. Here the porphyrin "hole" assumes its important role and provides a low energy level that can accept the excess electron (in σ^*_{CO}) and prevent excessive energy rise. This role is similar to the effect noted[46] for the empty dangling orbitals of the bare FeO^+ in gas-phase hydroxylations.[47] *Thus, the porphyrin "hole" serves as an electronic sink which facilitates the formation of the hydroxylation products*. This conclusion provides theoretical support for the findings[48] that Compound II-type ferryls with a closed-shell porphyrin either do not exhibit an oxidative activity[48a] or are sluggish oxidants which give a high degree of nonstereospecificity.[48b]

The "Push Effect" of the Proximal Ligand. The electron sink ("a_{2u} hole") may not be sufficient by itself to eliminate a rebound barrier, since the making of the C−O bond is attended by Fe−O bond elongation (Scheme 6a). We recall that such

(45) For similar considerations, see: (a) Zakharieva, O.; Grodzicki, M.; Trautwein, A. X.; Veeger, C. Rietjens, I. C. M. *Biophys. Chem.* **1998**, *73*, 189−203. (b) Grodzicki, M.; Trautwein, A. X.; Veeger, C.; Rietjens, I. C. M. *J. Inorg. Biol. Chem.* **1996**, *1*, 192−204.

(46) Filatov, M.; Shaik, S. *J. Phys. Chem. A* **1998**, *102*, 3835−3846.

(47) For a review of FeO^+ reactivity, see; Schröder, D.; Schwarz, H. *Angew. Chem., Int. Ed. Engl.* **1995**, *34*, 1973−1995.

(48) (a) Kamaraj, K.; Bandyopadhyay, D. *J. Am. Chem. Soc.* **1997**, *119*, 8099−8100 (especially footnote 13 therein). (b) See ref 37.

effects are associated with the barrier in the HS rebound. Therefore, a second factor is required to mitigate the effect of the Fe−O elongation and eliminate the LS rebound barrier, and this factor is the shortening of the Fe−S bond between the iron and the proximal ligand (shown in Scheme 6a). A simplified orbital picture of this effect is shown in parts (c) and (d) of Scheme 6. Thus, as shown in (c), the Fe−O bond elongation during the LS rebound lowers the $\sigma^*(d_{z^2})$, which is Fe−O antibonding (see bold arrow), and hence its interaction with the p_σ(S) orbital gets stronger, thereby shortening the Fe−S bond (see bold arrow). As the Fe−S bond gets shorter, the π-back-bonding of the thiolate to the iron will also become more significant and further strengthen the Fe−S bond, due to the orbital interaction between the p_π(S) orbital and the $\pi(d_{yz})$ Fe orbital, shown in Scheme 6d.[36c] These Fe−S orbital interactions mitigate of the Fe−O bond lengthening and prevent a barrier in the LS rebound process.

This role of the Fe−S bond shortening can be associated with the well-known "push effect" of the thiolate ligand and with the general conclusion that thiolate acts as a strong "internal donor".[2,5,6,36c,45,49,50,51] It is apparent, therefore, that the thiolate ligand plays opposing roles in the HS and LS rebound processes. *In the HS rebound, the Fe−S bond elongates due to the population of the $\sigma^*(d_{z^2})$ orbital. In contrast, in the LS rebound, the Fe−S bond shortens and mitigates the effect of Fe−O bond lengthening, thereby creating an effectively concerted hydroxylation, albeit with two different phases which resemble distinct steps.*

B. A Relationship of Computed Two-State Reactivity to Experimental Data. What can be learned from the foregoing two-state reactivity (TSR) scenario, on the question of the lifetime of a free radical in the rebound mechanism? First, one needs to ascertain that a free radical can, indeed, be formed in the rebound mechanism. While it is not possible to rule out the generation of radicals from the LS process, the computational results clearly indicate that such a species may occur primarily on the HS surface, which exhibits a significant barrier to rebound. Figure 3 shows that the separation of the ^4C_I intermediate to ferryl-hydroxo plus free methyl radical is extremely facile, ca. 2 kcal/mol, and smaller than the barrier to rebound. With such a small binding energy of the methyl radical, one should expect that entropy effects would shift the equilibrium in favor of the free radical. Indeed, on a free energy scale the ^4C_I cluster is 3.6 kcal/mol higher than the separated iron-hydroxo complex and the free methyl radical. Clearly such a radical species may find sufficient time to rearrange, provided it is a fast enough clock. Alternatively, since the binding of the radical is so feeble, an in-cage rearrangement can take place in competition with rebound.[52]

Scheme 7. A Simplified Two-State Rebound Mechanism[a]

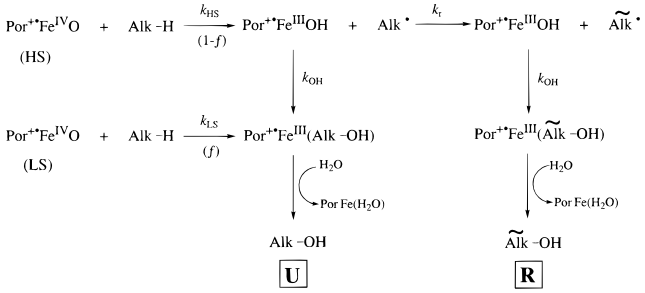

[a] Alk is an alkyl group.

B.1. Why Do Lifetimes of Radical Clocks Appear Too Short? Since the computed LS rebound is effectively concerted, the amount of radicals generated from the LS path can be neglected, in comparison with the radical concentration generated from the HS process (the HS excess is ca. 1000-fold, considering the barrier height). It is clear, therefore, that the apparent lifetime of the radical determined from the rearrangement data does not actually measure the radical lifetime, since rearranged products can arise only from the HS process, while unrearranged products arise from both HS and LS processes. To model this more quantitatively, we constructed the simplest kinetic scheme on the basis of the TSR scenario, as shown in Scheme 7, where complications such as clusters, details of spin crossovers, reversibility, and so on are avoided. The TSR scheme is based on the fractionation (e.g., by spin crossover[40] or spin state equilibration) into two otherwise parallel pathways: one HS and one LS. The HS path enables the radical to escape and form both rearranged products (indicates by a wiggle over the alkyl group) labeled as [R] and unrearranged products labeled as [U]. In contrast, the LS process is effectively concerted, leading only to [U] products. With this simple scheme, the TSR rate constant for rebound is given in eq 1, where K depends on

$$k_{OH}^{(TSR)} = k_r([U/R] - K)/(1 + K); \quad K = [f/(1 - f)]k_{LS}/k_{HS} \tag{1}$$

the fractionation into the LS path (fraction f) and the HS path $(1 - f)$ and on the ratio of the LS and HS rate constants for the bond activation. [U/R] is the observed ratio of unrearranged to rearranged products, and k_r is the rate constant of free radical rearrangement.

The corresponding apparent rate constant is determined simply from the [U/R] quantity[12−17] without the TSR scenario as shown in eq 2. Comparison of the two expressions for k_{OH}

$$k_{OH}^{(app)} = k_r([U/R]) \tag{2}$$

shows that the apparent rate is smaller than the corresponding value from the TSR scenario (eq 1). Since the radical lifetime (τ) is inversely related to the rate constant, the "real" lifetime based on TSR is always longer than the apparent lifetime, as shown in eq 3.

$$\tau^{(TSR)}/\tau^{(app)} = [(U/R)(1 + K)]/[(U/R) - K] > 1; \quad K = [f/(1 - f)]k_{LS}/k_{HS} \tag{3}$$

(49) (a) See discussion in ref 6a. (b) Traylor, T. G.; Traylor, P. S. In *Active Oxygen in Biochemistry*; Valentine, J. S., Foote, C. S., Greenberg, A., Liebman, J. F., Eds.; Blackie Academic & Professional: New York, 1995; Chapter 3, pp 84−187.

(50) (a) Bernadou, J.; Fabiano, A.-S.; Robert, A.; Meunier, B. *J. Am. Chem. Soc.* **1994**, *116*, 9375−9376. (b) Dawson, J. H.; Sono, M. *Chem. Rev.* **1987**, *87*, 1255−1276. (c) Champion, P. M. *J. Am. Chem. Soc.* **1989**, *111*, 3433−3434. (d) Bangcharoenpaurpong; Champion, P. M.; P. M.; Martinis, S. A.; Sligar, S. G. *J. Chem. Phys.* **1987**, *87*, 4273−4284. (e) Liu, H. S.; Sono, M.; Kadkhodayan, S.; Hager, L. P.; Hedman, B.; Hodgson, K. O.; Dawson, J. H. *J. Biol. Chem.* **1995**, *270*,10544−10550. (f) Staubli, B.; Fretz, H.; Piantini, U.; Woggon, W.-D. *Helv. Chim. Acta* **1987**, *70*, 1173−1193. (g) Czernuszewicz, R. S.; Su, Y. O.; Stern, M. K.; Macor, K. A.; Kim, D.; Groves, J. T.; Spiro, T. G. *J. Am. Chem. Soc.* **1988**, *110*, 4158−4165. (h) See discussion in ref 36c.

(51) For recent discussion of the thiolate "push effect" and the role of hydrogen bonding therein, see: (a) Roach, M. P.; Pond, A. E.; Thomas, M. R.; Boxer, S. G.; Dawson, J. H *J. Am. Chem. Soc.* **1999**, *121*, 12088−12093. (b) Sigman, J. A.; Pond, A. E.; Dawson, J. H.; Lu, Y. *Biochemistry* **2000** *38*, 11122−11129.

(52) In fact, the gas-phase calculation is geared toward clusters, but their presence under real conditions may be questionable. In solution, it is very likely to expect a free radical out of cage. In the protein pocket the radical may detach itself from the ferryl-hydroxo and form weak clusters with moieties in the pocket.

The disparity between the two values of the lifetime depends on the K quantity. The larger the K, the greater the disparity, and the shorter will be the apparent lifetime derived from eq 2, relative to the TSR quantity (eq 1). Even if we assume $K = 1$, the TSR lifetime is approximately double the apparent lifetime. Doubling the reported[17e] apparent lifetimes of the radical clocks leads to radical lifetimes of 160−400 fs, which are already quite reasonable values for an intermediate. In fact, even lower values (of 140 fs) were shown recently[53] to enable the trimethylene diradical to perform internal rotations. In practice, K may be larger than unity (see later), and therefore the TSR lifetimes of the radical in the two-state rebound would not be very short, if such values could be measured.

Thus, we are in agreement with Newcomb et al.[17e] that once the mechanistic scheme diverges from the simple rebound mechanisms, the measurement of [U/R]) for radical clocks can no longer be used to gauge the radical lifetime. It follows, therefore, that the TSR scenario provides a plausible explanation for the result that the apparent lifetimes can be too short, and still radicals may be present. However, *the TSR scenario increases the free radicals' lifetime to acceptable values and provides a simple rationale for the partial scrambling (e.g., unequal scrambling in allylic positions) which is observed in stereochemical studies*. Thus, the two-state scenario reconciles the apparent contradiction between the fast-clock data,[17] which appear inconsistent with either free radical intermediary or the rebound mechanism, vis à vis scrambling data[20−22] and kinetic isotope effect profiles,[16] which support both the presence of radicals and the rebound mechanism.

C. Predictions of Reactivity Patterns in a Two-State Rebound Mechanism. Let us now analyze the factors which determine the barriers in the various pathways of the rebound mechanism, based on the discussion in the preceding sections.

Reactivity Patterns in the Hydrogen Abstraction Phase. The analogy of the bond activation phase to a hydrogen abstraction reaction (Scheme 3) indicates that, much as in simple hydrogen abstraction reactions,[42a,54] here too the major factors which will determine bond activation reactivity for a given isozyme with a series of alkanes will be the C−H bond energy and the donor ability of the alkane. The weaker the bond and the better donor is the alkane, the lower would be the barrier for H abstraction in both HS and LS pathways. Although the experimental data are indicative of such a general selectivity to hydroxylate weaker bonds and substrates which are better donors,[1,2] this trend is not easy to test by experiment, because the oxidation step is not the rate-determining step in the catalytic cycle of the enzyme. We hope that model systems can establish these trends.

Reactivity Patterns in the Rebound Phase. Three factors will affect the height of the HS rebound barrier:

(i) The first factor is associated with the rebounding alkyl radical which gets oxidized; the better donor the alkyl radical, the smaller will be the rebound barrier. Since the barrier is not large to begin with, it may eventually vanish for good donors.

(ii) The second factor is associated with the height of the $\sigma^*(d_{z^2})$ orbital, which in turn depends on the σ-donor ability of the thiolate ligand. The better σ-binder is the thiolate, the higher is the $\sigma^*(d_{z^2})$ orbital and the larger will be the rebound barrier.

(iii) The third factor is the strength of the forming C−O bond, which determines the thermodynamic driving force of the rebound step.

While a systematic structure−reactivity pattern of these factors may not be easy to achieve, the ratio of rearranged to unrearranged alcohol, [U/R], is an experimentally testable quantity. A useful expression, based on the TSR scenario in Scheme 7, is given in eq 4, and is simply the sum of the rates

$$[\mathrm{U/R}] = [K + k_{OH}/(k_r + k_{OH})]/[k_r/(k_r + k_{OH})]; \quad K = [f/(1 - f)]k_{LS}/k_{HS} \quad (4)$$

of producing unrearranged [U] alcohol from both HS and LS pathways, divided by the rate of producing rearranged [R] alcohol from the HS path. At the limit of $k_{OH}/k_r \gg 1$, the quantity [U/R] is very large; namely, little or no rearrangement will be detected. Experimentally, for clocks with $k_r < 10^9$ s^{-1}, no rearrangement products were detected.[8,11c,12] At the other limit, for very fast clocks ($k_r \gg k_{OH}$), one gets simply [U/R] = K; i.e., the ratio of unrearranged to rearranged alcohol product will depend on the fractionation of the HS and LS paths, given by $[f/(1 - f)]$, and the ratio of their rates of hydrogen abstraction (k_{LS}/k_{HS}). In this case, the [U/R] ratio will exhibit no correlation with the free radical lifetime ($1/k_r$). The experimental situation with fast clocks seems to behave in a similar fashion.[17a]

Between the two limits, [U/R] will depend, as per eq 4, on both the HS and LS rates in the hydrogen abstraction (k_{LS}/k_{HS}) phase as well as on the HS rebound rate (k_{OH}) relative to the rate of free radical rearrangement (k_r). We can now use this idea to make some predictions about expected structure−rearrangement patterns.

The present results for methane activation (Figure 1) show that the high-spin and low-spin barriers for hydrogen abstraction are close in energy. However, the charge distribution data in Figure 4 show that the ^2TS_H species involves a slightly higher degree of charge transfer from methane to the ferryl-oxene unit, in comparison with the ^4TS_H species. It is likely, therefore, that as the alkane becomes a better electron donor, the ^2TS_H will be preferentially more stabilized, thereby preferring the low-spin process over the high-spin path. Based on eq 4, this factor by itself will lower the percentage of rearrangement and increase the [U/R] ratio. The second factor is the donor property of the rebounding radical, which gets oxidized during the rebound. As the radical becomes a better electron donor, the rebound barrier will become lower, thus increasing k_{OH}^{TSR} and decreasing the percentage of radical rearrangement. It follows, therefore, that as both the alkane and its hydrogen-abstracted radical become better electron donors, the amount of radical rearrangement will decrease quite fast. In fact, at some point the HS rebound will become barrierless itself, and no rearrangement will be observed.

The above prediction can be compared with the experimental data of Newcomb et al.[17c] in Scheme 8. The substrates are arranged in the scheme in order of increasing donor property, and it is apparent that as the substrate and the corresponding hydrogen-abstracted radical become better electron donors the [U/R] ratio increases, and for the best donor substrate virtually no rearrangement could be detected. A similar trend can be found in the data of Bowry and Ingold,[12a] where the highly methylated cyclopropanes (and hence the better donor ones) were found to exhibit low percentages of rearrangement. While these trends follow the TSR predictions, a full structure−reactivity study of clocks can reveal the interplay of the donor properties of the alkane, the radical, and the C−O bond strength

(53) Hrovat, D. A.; Fang, S.; Borden, W. T.; Carpenter, B. K. *J. Am. Chem. Soc.* **1997**, *119*, 5253−5254. The paper shows that a lifetime as short as 140 fs is sufficient for stereomutation of the trimethylene diradical.

(54) For a discussion of these factors, see: Shaik, S.; Shurki, A. *Angew. Chem., Int. Ed.* **1999**, *38*, 586−625.

Scheme 8. Radical-Type Rearrangement Data (from Ref 17c)

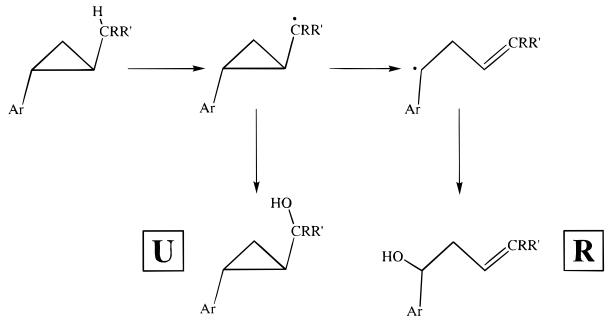

Ar	R, R'	[U/R]
p-CF_3	H, H	4
p-H	H, H	4.3
p-CF_3	H, CH_3	12
p-H	H, CH_3	25
p-H	CH_3, CH_3	>100

in the forming alcohol. Of course, rearrangement products due to cationic intermediate must be excluded properly, as done by Newcomb et al.[17e]

Rebound Reactivity Patterns Due to the Proximal Ligand Effect. Another factor which determines the HS rebound rate constant k_{OH} is the energy level of the $\sigma^*(d_{z^2})$ orbital which becomes populated during the HS rebound. This factor will be controlled by the encapsulating protein, which can affect the binding of the thiolate via steric constraints as well as via the hydrogen-bonding capability (acidity) and/or effective polarity of its pocket.[36b,c,51] Thus, it is expected that different isozymes will have different rebound barriers. The more acidic the protein pocket and the more constrained the thiolate binding, the lower will be the rebound barrier, and less rearrangement is expected in the HS process.[55] The experimental data[23] are not conclusive enough to allow us to claim much, if anything. But the prediction stands to a test which may affirm the model or lead to its revision and refinement.

Conclusion

The ferryl-oxene active species (Compound I)[4,7,8] is a two-state reagent, having closely lying quartet and doublet states. A DFT investigation of the rebound mechanism, in a model alkane hydroxylation, shows that these two states are competitive. As such, alkane hydroxylation by Compound I is a two-state reactivity (TSR) scenario, whereby reactivity patterns and product distribution are determined by the interplay of the two states.

The reaction mechanism consists of two phases: a bond activation phase, responsible for the C−H cleavage by Compound I, and a rebound phase, whereby the alkyl residue makes a C−O bond and generates the ferric−alcohol product complexes. The transition states for the bond activation phase, $^{2,4}TS_H$, are hydrogen abstraction transition states in which the moiety O−C−H possesses geometry and electronic structure that are virtually identical to those of a model transition state for a hydrogen abstraction by an alkoxy group (Scheme 3). *Thus, the contention of Dinnocenzo and Jones,[16] that the bond activation by P450 can be modeled using a simple hydrogen abstraction by an alkoxy radical, is quite reasonable.* Detailed kinetic isotope effect calculations will be needed, though, to explore the full mechanistic significance of the Dinnocenzo−Jones method.

The high-spin (HS) quartet-state hydroxylation is stepwise, and past the hydrogen abstraction phase, the intermediate cluster of iron-hydroxo and the alkyl radical, ^4C_I, undergoes rebound with a distinct transition state, $^4TS_{reb}$, and a barrier. The ^4C_I cluster is weakly bound (ca. 2 kcal/mol) and can easily release the radical. In contrast, the low-spin (LS) doublet-state hydroxylation is effectively concerted, whereby the corresponding intermediate cluster collapses without a significant barrier to the LS ferric−alcohol product. The facility of the LS rebound is due to two factors: the porphyrin "hole", which acts as an electron sink that accepts the excess electron in the forming C−O linkage, and the "push effect"[2,36c,50,51] of the thiolate ligand, which by shortening the Fe−S bond length during the rebound mitigates the effect of Fe−O bond lengthening. *The effectively concerted LS pathway accords with Newcomb's conclusion, that hydroxylation appears to proceed by a non-synchronous but an effectively concerted oxygen insertion reaction.*

Since there exists a weakly bound ^2C_I cluster, we cannot rule out incursion of free radical intermediate in the LS rebound. However, the computational results clearly show that the main source of the free radical, which can undergo rearrangement and generate rearranged alcohol products, is the HS state. Since unrearranged products are nascent from both HS and LS processes, while rearranged products arise only (or virtually so) from the HS process, this dichotomy of the rebound phase manifests as a too-short lifetime of the radical intermediates.[17c,e] The lifetime derived from the TSR scenario, if it could be measured, would be at least twice as long (see eq 3). *Thus, the Groves rebound mechanism is corroborated albeit in a two-state scenario which seems to be the root cause of the controversial behavior of the rearrangement data*[17] *and for the incomplete scrambling often observed in stereochemical probes.*[4,8,20]

Based on the TSR model and consideration of electronic structure features, some predictions are made regarding the factors which control the reactivity patterns in alkane hydroxylation. The weaker the C−H bond and the better electron donor is the alkane, the lower would be the barrier for the hydrogen abstraction. While this is a normal trend expected for hydrogen abstraction reactions,[35,42a,54] in the present TSR scenario the LS process is expected to benefit more from the improved donor property of the alkane.

The barrier for the HS rebound is predicted to decrease as the R$^\bullet$ becomes a better electron donor, the C−O gets stronger, and the proximal ligand becomes a weaker binder. Thus, in a series where the radical becomes an increasingly better electron donor, while other factors change less, the HS rebound barrier will gradually decrease, and *the HS process will eventually become effectively concerted*. The documented rearrangement trends of fast clocks[17c] seem to fit this prediction. The dependence of the rebound barrier on the binding ability of the proximal ligand is submitted for a test. Thus, the TSR scenario of the rebound mechanism reconciles a few conflicting findings[16,17,20,21] and makes new testable predictions.

There remain quite a few features of the hydroxylation mechanism by Compound I which require further study. First is the puzzling observation[17d,e,23a] that on one hand, substitution

(55) For related observations where the donor property of the ligand affects hydroxylation reactivity patterns, see: (a) Gross, Z.; Nimry, S.; Simkhovich, L. *J. Mol. Catal.* **1996**, *113*, 231−238. (b) Gross, Z.; Nimry, S.; Barzilay, C. M.; Simkhovich, L. *J. Bioinorg. Chem.* **1997**, *2*, 492−506.

of the methyl group in phenylmethylcyclopropane by deuteriomethyl (CD_3) exhibits a significant isotope effect, diverting the reaction from methyl to phenyl hydroxylation. On the other hand, the ratio of unrearranged to rearranged alcohol products due to the methyl hydroxylation remains constant and shows no isotope effect. In terms of the present results, this could be accounted for by invoking an identical isotope effect on the LS and HS hydrogen abstraction phases. A study of the isotope effects for the rebound mechanism is required and forthcoming.

A second important feature is the electronic structure of the iron-hydroxo intermediate (**2** in Scheme 1). The σ-donor ability of the thiolate and the polarization effect of the protein medium prefer the ferric form, $Por^{+\bullet}Fe^{(III)}OH$. Our preliminary results suggest that the HS rebound barrier for the $Fe^{(IV)}$ state is smaller than that for the $Fe^{(III)}$ state by ca. 2 kcal/mol. In addition, the sulfur-localized states (Figures 1 and 2) may become important as the π-donor property of the thiolate ligand increases. The merging of these aspects with the present results will certainly create a fascinating multistate scenario.

Finally, a test of the reactivity patterns due to the PorFeOOH oxidant would be required to understand the P450 hydroxylation in the broader sense, as indeed demonstrated by the studies of Newcomb et al.[17,23a] However, even with the second oxidant, a few states will still have to be considered. This, and the study of the proximal ligand effect on the fractionation of the HS/LS states and the oxidants, will certainly require a future QM/MM study.

Acknowledgment. This work is dedicated to Lennart Eberson, a great scientist, on his untimely death. This research was supported by the Israeli Science Foundation (ISF), and in part by the Volkswagen Stiftung. S.S. thanks the Humboldt Foundation for a Senior Research Award. F.O. thanks the EU for a Marie Curie Fellowship. S.S. thanks J. P. Dinnocenzo for a discussion of the TSR kinetic scheme and its implications. Very useful discussions with him, and with J. T. Groves, M. Newcomb (who also communicated ref 17e prior to publication), and J. P. Jones, are acknowledged.

Supporting Information Available: An archive document, containing Cartesian coordinates and absolute energies on the calculated species (PDF). This material is available free of charge via the Internet at http://pubs.acs.org.

JA991878X